Journal of Pure and Applied Sciences (JPAS),
Volume 2, Issue 2, Page 1-18, 2026

Investigation on the Antifungal potentials of Bioash-doped ZnO Nanocomposites prepared by Chemical Bath Deposition Technique for Biomedical applications

E. C. Oroke[1*], J. B. Owabumoye[2], O. M. Afuwape[3]

[1,3]Department of Applied Chemistry, The Federal Polytechnic Ado-Ekiti, Ekiti State, Nigeria.
[2]Department of Microbiology, The Federal Polytechnic Ado-Ekiti, Ekiti State, Nigeria
[1]oroke_ec@fedpolyado.edu.ng , [2]owabumoye_jb@fedpolyado.edu.ng , [3]afuwape_om@fedpolyado.edu.ng
*Corresponding author (Email: oroke_ec@fedpolyado.edu.ng, Phone: +2348065340090)

ABSTRACT

This study evaluated the antifungal efficacy of oil palm finger bioash-supported ZnO Nanocomposites (OPfBA-ZnO NCs) synthesized via chemical bath deposition as a sustainable nanomaterial for dermatophytosis management. The bioash and nanocomposites were characterized using EDX, Brunauer-Emmett-Teller (BET), UV–Vis, Raman, and Fourier transform infrared (FTIR) analyses. Antifungal activity was assessed against eight clinically important dermatophyte species. EDX revealed that the bioash contained abundant K (42.5 wt%), Ca (18.97 wt%), Si (5.33 wt%), and Ag (2.15 wt%), while BET confirmed a mesoporous structure (155.9 m^2/g; pore diameter ≈2.13 nm). The NCs exhibited pH-dependent optical properties with bandgap energies of 3.48–4.10 eV. Raman and FTIR analyses confirmed successful integration of bioash constituents into the ZnO matrix. The OPfBA-ZnO NCs showed broad-spectrum antifungal activity with inhibition zones of 10.11–26.80 mm, while the bioash alone produced 13.13–30.87 mm. The eco-friendly OPfBA-ZnO nanocomposite demonstrated promising anti-dermatophytic activity and potential for topical antifungal, antimicrobial coating, and environmental remediation applications.

***Keywords*— ZnO, Bioash, Nanocomposites, Antifungi, Doping**

I. INTRODUCTION

The rising global burden of fungal infections, compounded by the emergence of antifungal-resistant strains, has intensified the search for alternative antimicrobial agents capable of circumventing conventional resistance mechanisms [1]. Fungal pathogens such as Candida albicans, Aspergillus niger, and Fusarium species are responsible for significant morbidity and mortality, particularly among immune-compromised populations, making the development of novel antifungal materials a pressing biomedical priority [2].

In recent years, metal oxide Nanocomposites have attracted considerable attention as broad-spectrum antimicrobial agents owing to their unique physicochemical properties at the nanoscale [3]. Among these, ZnO NCs stand out as a particularly promising candidate for biomedical applications due to their wide bandgap (~3.37 eV), high exciton binding energy (60 meV), excellent biocompatibility, and intrinsic antimicrobial activity [4]. ZnO has been classified as a "generally recognized as safe" (GRAS) material by the United States Food and Drug Administration, further underscoring its suitability for therapeutic and biomedical use [5].

The antifungal efficacy of ZnO NCs has been demonstrated against a range of pathogenic fungi, including Candida albicans, Aspergillus flavus, Aspergillus fumigatus, and Penicillium species [6]. The primary mechanism underlying this activity involves the generation of reactive oxygen species (ROS), including superoxide anions, hydroxyl radicals, and singlet oxygen, which induce oxidative stress, lipid peroxidation, membrane disruption, and ultimately cell death in fungal organisms. Lipovsky et al. [7] demonstrated that the antifungal action of ZnO NCs against C. albicans is substantially mediated by ROS, with near-complete elimination of antifungal activity upon addition of ROS quenchers. Djearamane et al. [8] further showed that ZnO NCs cause dose-dependent morphological alterations on C. albicans cell surfaces, including hyphal damage, cell wall pitting, and membrane rupture.

A key strategy for enhancing the antimicrobial performance of ZnO NCs is doping, which is the deliberate introduction of foreign ions into the ZnO crystal lattice. Doping modifies the electronic band structure, increases lattice defects and oxygen vacancies, and enhances ROS generation, thereby amplifying antimicrobial activity. Several studies have demonstrated the efficacy of this approach using transition metals and rare earth elements as dopants. Ding et al. [9] reported that tantalum-doped ZnO Nanocomposites exhibit significantly improved bactericidal efficacy compared to pure ZnO, attributed to enhanced surface bioactivity and increased electrostatic interactions. Manganese-doped ZnO NCs has been documented to display superior antimicrobial activity compared to undoped ZnO, with minimum lethal concentrations as low as 40 µg/mL against E. coli and C. albicans [10]. Ogwuegbu et al. [11] recently reported that cobalt-doped ZnO NCs synthesized via a green route exhibited enhanced antifungal properties against Aspergillus niger, Mucor mucedo, and Penicillium chrysogenum, with minimum inhibitory concentrations as low as 0.03 mg/mL. These findings collectively establish that the choice of dopant plays a critical role in modulating the structural, optical, and biological properties of ZnO nanostructures.

While metallic and rare-earth dopants have been widely explored, the use of bioash, the mineral residue obtained from the combustion of biomass — as a dopant source remains largely uninvestigated. Bioash is an abundant, low-cost waste product rich in essential elements such as potassium, calcium, magnesium, phosphorus, and various trace metals, whose composition varies with biomass feedstock. The incorporation of bioash-derived elements into the ZnO matrix presents a novel and sustainable approach that simultaneously addresses the dual challenges of waste valorization and functional nanomaterial development. Biomass-derived precursors rich in phosphorus, nitrogen, and other heteroatoms can serve as effective green dopants for ZnO, enhancing visible-light absorption and modifying electronic properties [12].

The synthesis technique also significantly influences the morphology, crystallinity, and functional properties of ZnO nanostructures. Chemical bath deposition (CBD) is a wet chemical method that operates at relatively low temperatures (typically below 100°C), requires minimal instrumentation, and enables controlled deposition of nanocrystalline materials with good reproducibility [13]. Controlling growth parameters such as pH, temperature, and precursor concentration, CBD allows fine-tuning of ZnO morphology from nano-flowers to nano-flakes with well-defined crystalline hexagonal structures [14] Koao et al. [15] further showed that CBD is amenable to the incorporation of dopant ions (e.g., Tb^{3+}) into the ZnO lattice, with systematic effects on grain size, optical properties, and luminescence. These attributes make CBD particularly attractive for the synthesis of doped ZnO Nanocomposites, as it facilitates uniform dopant incorporation under mild aqueous conditions that are compatible with the dissolution of bioash constituents.

Despite the extensive literature on ZnO NCs and their antimicrobial applications, a significant research gap exists at the intersection of bioash doping, chemical bath deposition synthesis, and antifungal evaluation for biomedical applications. The present study therefore investigates, the antifungal potentials of bioash-doped ZnO Nanocomposites prepared by the chemical bath deposition technique. The structural, morphological, and optical properties of the synthesized Nanocomposites and the dopant were characterized, and their antifungal activity is evaluated against clinically relevant fungal pathogens. This work aims to contribute a sustainable, cost-effective nanomaterial platform with enhanced antifungal properties for potential biomedical applications, while simultaneously demonstrating the viability of biomass waste-derived materials as functional dopant sources in nanotechnology.

II. MATERIALS AND METHODS

A. Sampling and preparation

Oil palm (elaeis guineensis Jacq.) fingers were collected from the Federal Polytechnic Ado-Ekiti community. The bioash was prepared, following the procedure adapted from our previous studies [16] except that pyrolysis temperature was increased to 250 ±1oC with a resident time of 30min. The sample was later kept in a dessicator for further characterization and use. Similarly, reagents, glass substrate and bath preparation methods were adapted from our previous study with slight modification [16].

B. Sample characterization

Optical properties of the dopant and the bioash-supported NCs were studied using Uv-visible spectrophotometer (Jenway, 7315 Spectrophotometer) at wavelength ranges 200 – 1000 nm. Structural and microstructural properties of both dopant and doped NCs were investigated using FTIR (Agilent technologies) at 4000 – 650 cm^{-1} and Raman spectrophotometer (ProRaman-L-785-BIS Ser. No.196166) respectively. Surface morphology and textural characteristics of the both samples were evaluated using SEM model Phenom ProX, by phenomWorld Einhoven, The Netherlands) and BET specific surface area analyzer (Quantadrome Nova 2200E BET) respectively.

C. Antifungal studies

Antifungal activity of prepared both samples were determined by using agar well dilution method as described by Marzher et al. [17]. Briefly, a 72 h old-cultured growth of fungal organisms was dislodged with 10 mL of 1 % Toluene solution to harvest the spores and form suspension that was adjusted to a density of 4 X 105 spores per mL compared with 0.5 McFarland standard. Mueller Hinton Agar was prepared according to manufacturer prescription. A 6 mm diameter and 4 mm depth was bored on the prepared Mueller Hinton Agar using cork- borer. A 0.1mL (100 µL) antifungal agent each was dispensed into the bored hole. The plates were incubated at room temperatures for 72 hours. The diameter inhibition zones were measured using graduated meter rule and mean diameter of the inhibition zones.

III. RESULTS AND DISCUSSION

A. Optical characterization

The UV–visible spectrum of the bioash (Figures 1a) exhibits a broad absorption profile, cutting across the UV and visible regions (≈250–1000 nm), with a pronounced peak around ~500 nm and secondary features near ~600–900 nm, indicating the presence of conjugated π–π* and n–π* electronic transitions associated with carbonaceous and oxygenated functional groups [18]. The strong absorption in the UV region suggests

high photon-harvesting capability, while the extended tail into the visible region reflects defect states and surface functionalities typical of bio-derived ash materials. Such optical behavior implies that FBfBA can effectively act as a sensitizer and defect-inducing dopant when incorporated into ZnO, reducing electron–hole recombination and enhancing light absorption into the visible range. This is particularly advantageous for antifungal activity, as improved charge separation promotes the generation of reactive oxygen species (ROS), which are critical for disrupting fungal cell membranes and metabolic pathways [19]. Additionally, the presence of surface functional groups can facilitate Zn^{2+} ion interaction and improve nanoparticle dispersion and adhesion to microbial surfaces. Beyond antifungal applications, these properties make FBfBA a promising dopant for photocatalysis, environmental remediation, and optoelectronic devices.

On the other hand, optimization studies were carried out at various deposition parameters to investigate the optimal deposition conditions and results presented in figures 1b and c. Figure 1b summarily show the effect change in pH on the properties of the as-deposited bioash-doped ZnO NCs. Except for pH 8 which absorbed in the visible region, all other films absorbed maximally in the Uv-region of the spectrum at 350 nm, indicating hypsochromic shift. This is also similar to what obtained for the samples doped with biochar-doped and also in the work reported by Casa et al., [20]. Shoulder of peak position around 350 nm gives evidence that the as-prepared particles are in the nanometer range [20]. Therefore, the red shift or absorption in visible region can be said to be due to certain defects like oxygen deficiency causing oxygen vacancy between zinc and oxygen interstitials [21].

All the as-deposited bioash doped ZnO NCs have wide bandgap energies (Figure 1c) in the range of 3.48 – 4.10 eV. This is similar to the values reported by Khan et al., [22] and has possible application in optoelectronic industries. Wide bandgap semiconductors with a bandgap especially the ones >3 eV offer possible solutions because the wider bandgap allows them to withstand rapid switching frequencies and high power loads while maintaining insulating properties. Additionally, wide bandgap semiconductors have the advantage of stability at high temperatures, working under high voltages and currents, and exhibit high carrier density and mobility. As we know, bandgap is the minimum amount of energy needed to free an electron from its bond, and differs depending on the semiconductor material. Hence, low band gap materials have the advantage of absorbing low-energy photons, whereas high band gap materials can use high-energy photons [22]. The improvement in the optical bandgap energies could be linked to our earlier submission of multiple metals doping, which either reduces or boosts the bandgap and properties [23].

Refractive index of the as-deposited films were in the range 2.44 – 2.64 (Figure 2a), which were in tandem with the range values reported by Bolarinwa et al., [24] and Hu, [25] respectively for oxygen-deficient and nearly stoichiometric ZnO. Figure 2b showed a continuous decrease of extinction coefficient with the increase in photon energy except for pH 9 and 10 which increased at photon energy of 4.13 eV and continuously dropped. However, the reverse was the case for optical conductivity (Figure 2d) which dropped at photon energy of 4.13 eV and then increased. Similarly, graph of the dielectric (Figure 2c) shows the same trend as that of the conductivity. The sharp increase in the conductivity and dielectric constant around the bandgap can be attributed to the strong interaction between the photon and electron. The optical dielectric constant is a marker for the attraction of grains to light [26].

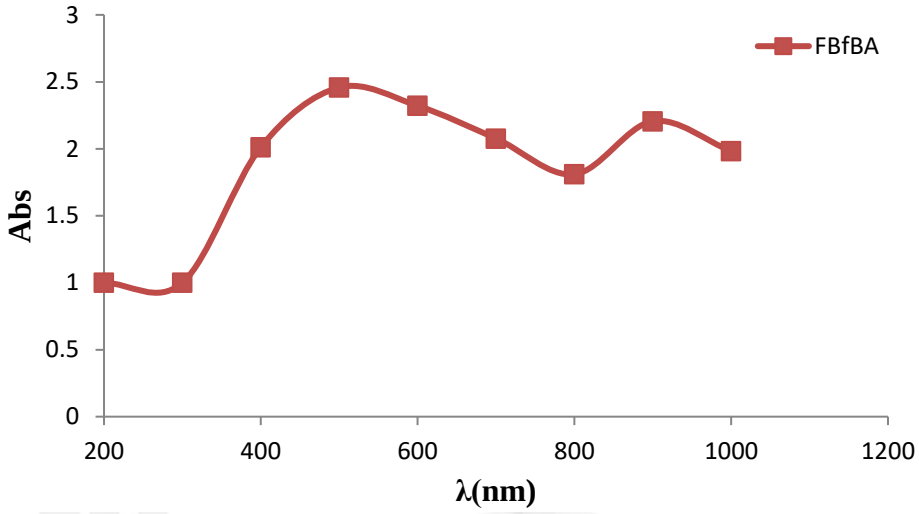

(a)

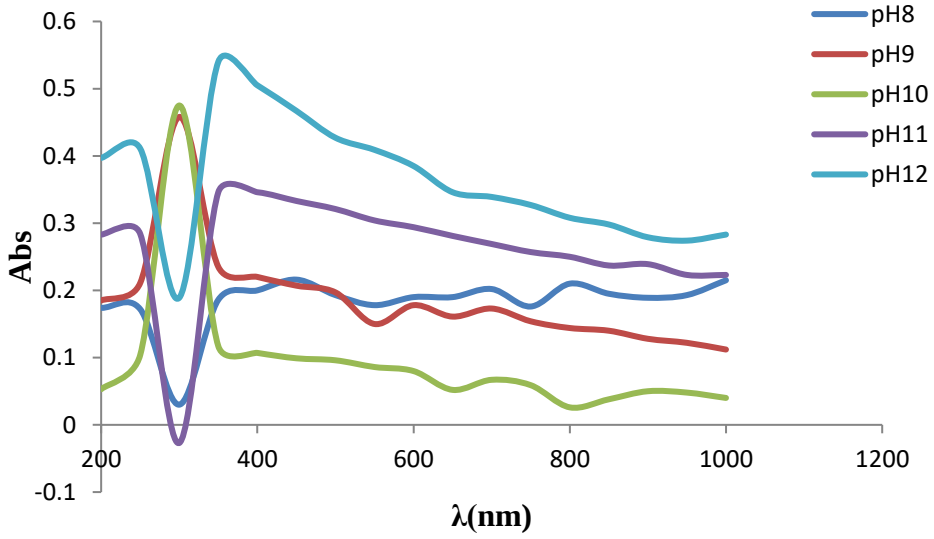

(b)

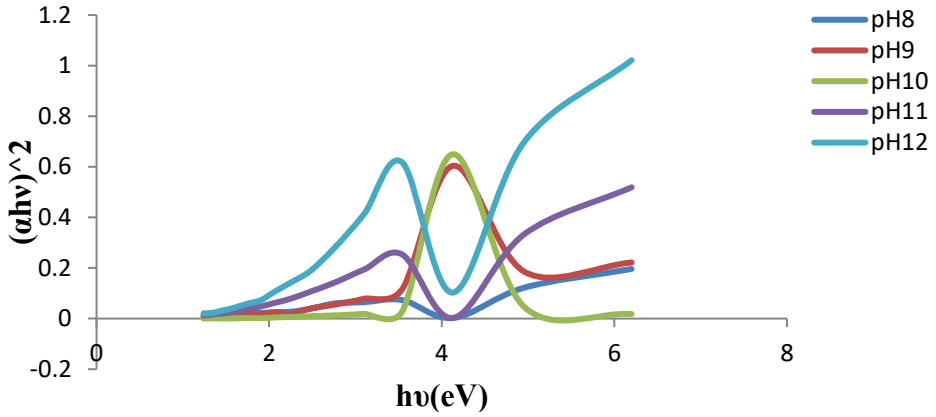

(c)

Figure 1: Plot of absorbance (a) Absorbance of the bioash-dopant (b) Doped ZnO NCs at different pH (c) Bandgap evaluation

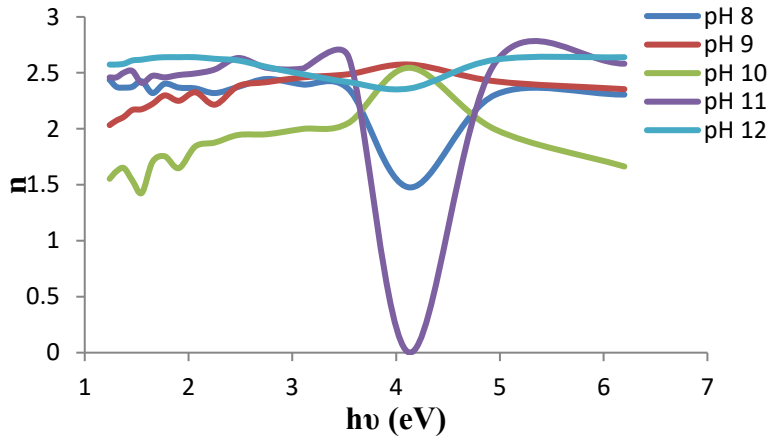

(a)

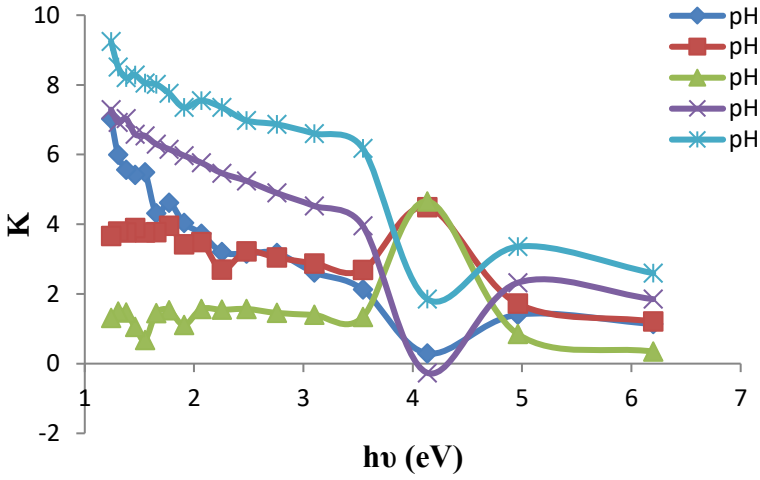

(b)

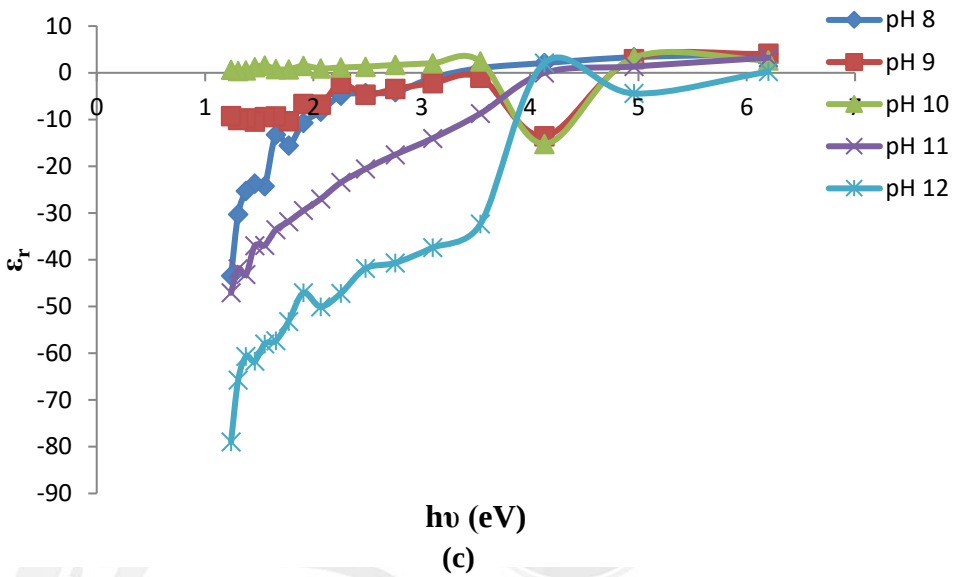

(c)

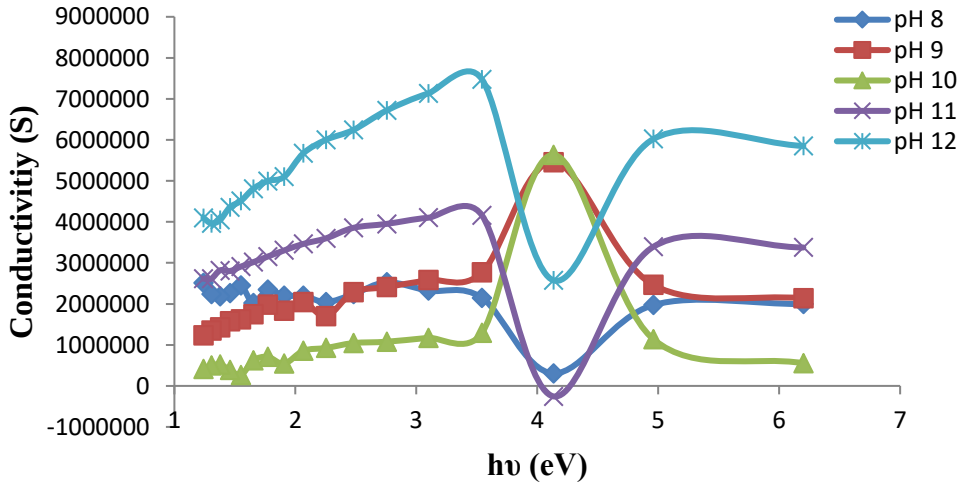

(d)

Figure 2: Plot of (a) Refractive index (b) Extinction coefficient (K) (c) Real dielectric constant (d) Optical conductivity spectra

B. Structural and microstructural analysis

The prepared bioash were characterized using FTIR so as to ascertain the organic functional groups and complexes present in the biomass by comparing the vibration frequencies in wave numbers of the sample spectrograph obtained from an FT-IR spectrophotometer with those of an IR correlation chart. The bioash showed strong vibrational bands at 2981.9 cm^{-1} and 2083.6 cm^{-1} corresponding to the existence of C-H and N=C=S stretching of alkane and isothiocyanate for FBBA. There was also a medium band at 1636.3 cm^{-1} which corresponds to the C=C stretching of conjugated alkenes. Other bands were found at 1457.4 cm^{-1},

1401.5 cm^{-1} and 990.3 cm^{-1} which are related to strong C-H bending of the alkyls, strong bending of S=O stretching (sulphonyl chloride) and C=C bending of alkene.

Figure 4 is the Raman spectrum of the bioash-supported ZnO Nanocomposites. Result show that it exhibited distinct vibrational features that confirm the successful formation of ZnO with bio-derived surface functionalities. The prominent high-intensity peak observed at ~2872 cm^{-1} is attributable to C–H stretching vibrations, indicating the presence of residual organic moieties from the bioash matrix. These surface-bound functional groups are crucial, as they can enhance nanoparticle stability and facilitate interaction with microbial cell membranes [27]. The band around ~1776 cm^{-1} can be assigned to C=O stretching vibrations, further supporting the incorporation of oxygenated functional groups from the bio-template.

In the lower wavenumber region, peaks around ~684 cm^{-1} and ~834 cm^{-1} are characteristic of Zn–O lattice vibrations, confirming the crystalline formation of ZnO. The peak near ~412 cm^{-1} corresponds to the E_2 (high) mode of hexagonal wurtzite ZnO, which is a signature Raman-active mode indicating good crystallinity and phase purity [28]. The relatively broad but discernible bands suggest nanoscale crystallite size and slight lattice distortions, likely induced by bioash incorporation. The coexistence of ZnO phonon modes and bioorganic functional groups demonstrates a successful hybrid structure, where the bioash not only acts as a support but also modifies the surface chemistry of ZnO Nanocomposites.

From an application standpoint, these structural and surface features strongly support the antifungal potential of the material. The nanoscale ZnO provides a high surface area for reactive oxygen species (ROS) generation, a key mechanism in antifungal activity [29]. Meanwhile, the bioash-derived functional groups enhance adhesion to fungal cell walls and may facilitate sustained release of Zn^{2+} ions. Additionally, the defect states implied by peak broadening can promote electron–hole separation, further boosting reactive oxygen species (ROS) production under ambient or photo-activated conditions. Overall, the Raman analysis confirms the formation of a structurally integrated, bio-functionalized ZnO nanocomposite with enhanced surface reactivity, making it a promising candidate for antifungal applications in biomedical and environmental systems.

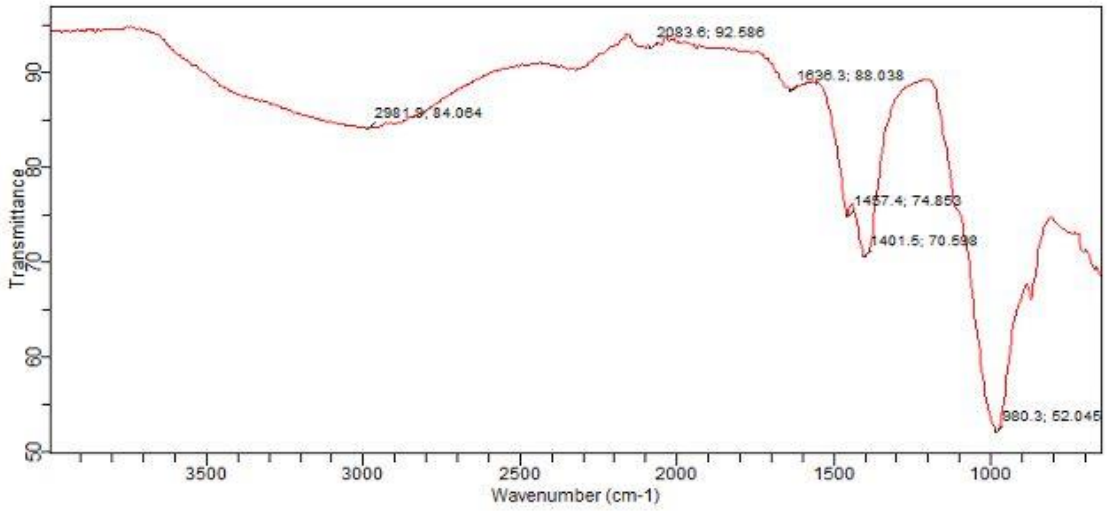

Figure 3: FTIR spectra of the Bioash-dopant

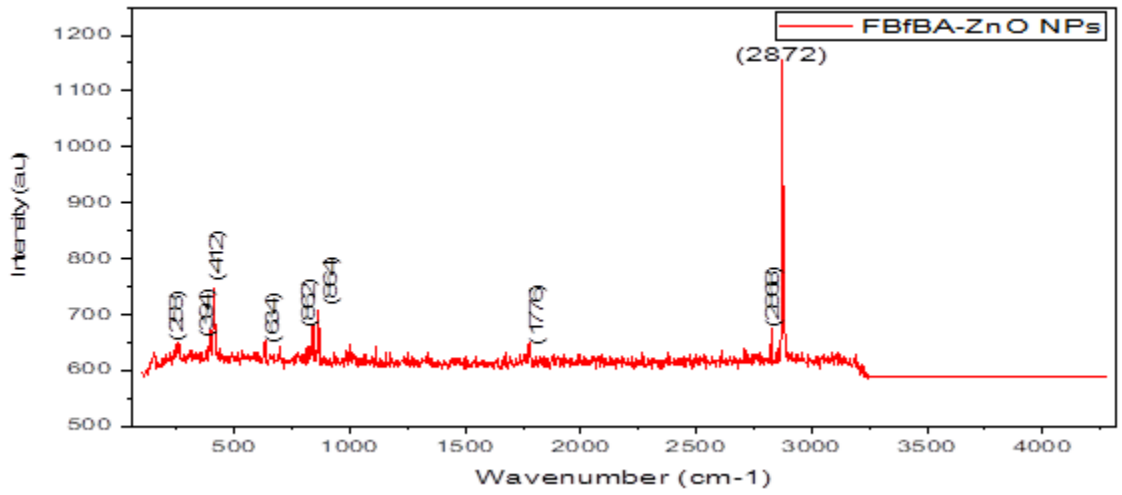

Figure 4: Raman Spectra of the as-deposited Bioash-doped ZnO NCs at pH 9

C. Elemental and surface morphology of the dopant

The EDX elemental composition of the oil palm fingers bioash reveals a mineral-rich dopant dominated by potassium (42.5 wt%), calcium (18.97 wt%), and chlorine (14.05 wt%), with notable amounts of silicon (5.33 wt%), phosphorus (3.82 wt%), zinc (2.31 wt%), and silver (2.15 wt%), alongside trace quantities of magnesium, aluminium, iron, sulphur, sodium, and carbon. This multi-element composition makes the bioash an exceptionally suitable support for ZnO NCs because the heterovalent cations, particularly Ca^{2+}, K^{+}, and Mg^{2+}; can substitute into or interact with the ZnO wurtzite lattice, creating crystalline defects such

as zinc vacancies, oxygen vacancies, and interstitial defects that enhance reactive oxygen species (ROS) generation, which is the principal mechanism of antifungal action. The presence of silver (2.15 wt%) is especially significant, as Ag doping in ZnO has been shown to synergistically amplify antimicrobial activity, with 5% Ag/ZnO identified as optimal for antifungal efficacy as it facilitates charge separation that boosts ROS production and releasing Ag^{+} ions that directly damage fungal cell membranes [30]. The silicon content (5.33 wt%) further adds value, as silica can form a protective coating on ZnO that improves colloidal stability and biocompatibility while maintaining antifungal efficacy, making the composite suitable for agricultural and biomedical applications [31]. Collectively, this naturally derived multi-element dopant profile eliminates the need for expensive synthetic precursors and provides a synergistic cocktail of antimicrobial, photocatalytic, and surface-modifying elements that render the bioash-doped ZnO NCs a cost-effective, eco-friendly, and potent antifungal nanocomposite with broad-spectrum applicability [32].

Table 1: EDX Elemental compositions of the Bioash-dopant

Element No	Symbol	Name	Sample and weight conc.
			FB_fBA
19	K	Potassium	42.5
6	C	Carbon	2.38
20	Ca	Calcium	18.97
17	Cl	Chlorine	14.05
14	Si	Silicon	5.33
15	P	Phosphorus	3.82
16	S	Sulphur	1.83
12	Mg	Magnesium	2.28
13	Al	Aluminum	0.29
8	O	Oxygen	0.41
11	Na	Sodium	0.12
26	Fe	Iron	0.36
47	Ag	Silver	2.15
30	Zn	Zinc	2.31
Others	-	-	3.90
Total	-	-	**100**

Figure 5 is the SEM micrograph of the bioash-dopant which revealed a highly heterogeneous, irregular morphology, composed of agglomerated particles with rough surfaces and an interconnected porous framework. The presence of micro- to meso-scale pores and fissures indicates incomplete carbonization and the retention of volatile-derived voids, which significantly enhance surface area and active site availability [33]. This textural complexity is advantageous for doping ZnO Nanocomposites, as it promotes strong interfacial anchoring, improved dispersion, and efficient charge transfer between the bioash matrix and ZnO. The porous and defect-rich structure can facilitate adsorption of oxygen and moisture, thereby enhancing reactive oxygen species (ROS) generation, a key mechanism underpinning antifungal activity [34]. Additionally, these structural attributes make the bioash a promising candidate for applications in photocatalysis, environmental remediation, adsorption of pollutants, and as a support material in energy storage systems.

D. N2 Adsorption

The BET surface area analysis of the oil palm fingers bioash, prepared via slow pyrolysis at 250°C for 30 minutes. Figure 6 reveals a moderate specific surface area of 155.9 m^2/g, a total pore volume of 0.076 cc/g, and an average pore diameter of 2.13 nm, which classifies it as a mesoporous material. This level of surface area, derived from the Type IV isotherm with a characteristic hysteresis loop (visible in the provided plot), suggests a well-developed porous structure composed primarily of mesopores, which is favorable for acting as a support or dopant [35]. The moderate surface area and mesoporous nature make this bioash highly suitable as a dopant for ZnO Nanocomposites, as it can provide abundant anchoring sites to prevent nanoparticle agglomeration and enhance the composite's active surface area for antifungal activity [36]. Furthermore, the carbon-rich and mineralized structure of such bioash can improve the charge separation and stability of ZnO under light irradiation, extending its potential applications to photocatalytic degradation of organic pollutants, gas sensing, and as a reinforcing filler in polymer composites.

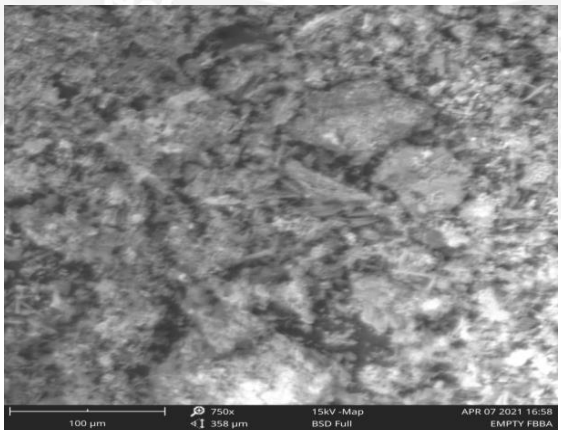

Figure 5: SEM Micrograph of the oil palm bioash-dopant

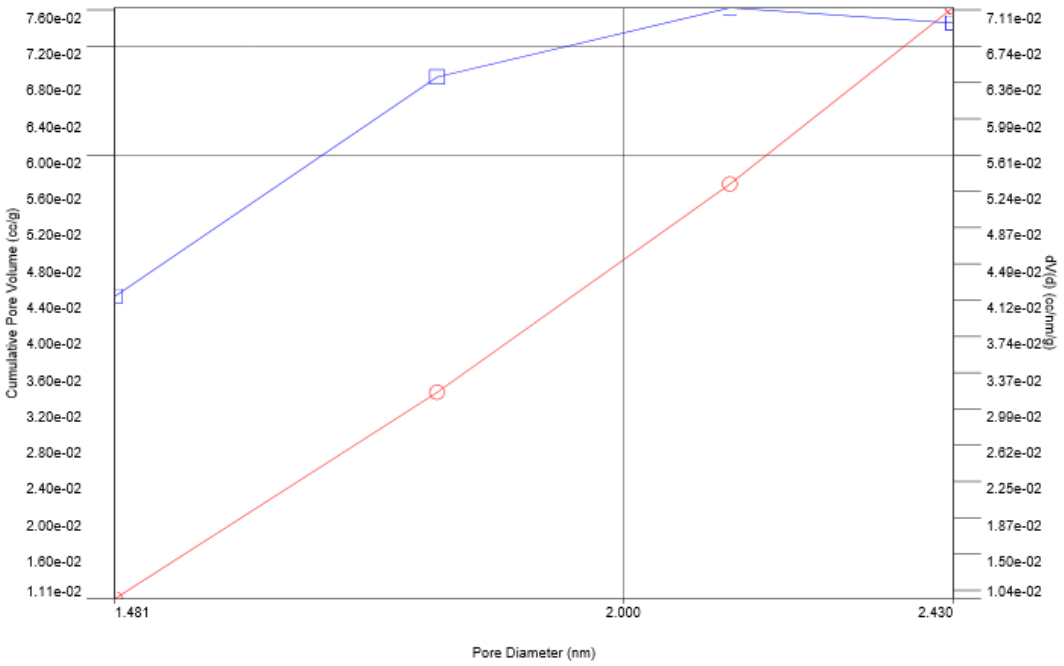

Figure 6: BET specific surface area plot of the empty Oil Palm Fruit bunch fingers bioash

E. Antifungal investigation

Table 2 reveals that both the bioash-doped ZnO NCs and the bioash-dopant exhibited appreciable antifungal activity against all eight tested dermatophyte species, with inhibition zone diameters ranging from 10.11 to 26.80 mm for the doped ZnO and 13.13 to 30.87 mm for the bioash alone. Notably, the bioash consistently produced larger inhibition zones than the bioash-doped ZnO NCs across all fungal species, suggesting that the mineral-rich bioash, which contains silica, potassium, calcium, and magnesium oxides, possesses intrinsic antifungal potency, likely attributable to its ultra-alkaline nature and direct ion-mediated disruption of fungal cell membranes. Both materials showed the strongest activity against Trichophyton schoenleinii (26.33 and 30.87 mm), T. mentagrophyte (26.80 and 28.60 mm), and T. rubrum (26.41 and 27.66 mm), which are clinically significant anthropophilic dermatophytes responsible for tinea capitis and tinea corporis, which are consistent with the known susceptibility of Trichophyton species to ZnO-based Nanocomposites. Conversely, T. violaceum (10.11 mm) and Microsporum canis (10.88 mm) were the least susceptible to the doped ZnO NCs, indicating species-dependent resistance that may relate to differences in cell wall composition and ergosterol content. The slightly reduced inhibition zones of the doped ZnO NCs relative to the bioash alone do not diminish their significance; rather, doping introduces the advantage of reactive oxygen species (ROS) generation and bandgap-tunable photocatalytic activity that the bioash lacks, enabling a dual-mechanism antifungal action (direct contact killing plus ROS-mediated oxidative

stress) particularly useful under UV or visible light exposure [37]. Overall, the inhibition diameters recorded, many exceeding 15 mm, compare favorably with values reported for other doped ZnO systems against dermatophytes and even standard antifungals like griseofulvin, confirming the therapeutic relevance of this bioash-doped ZnO nanocomposite [38]. These results support the potential application of the bioash-doped ZnO NCs not only as topical antifungal agents against dermatophytosis, but also in antibacterial textile coatings, photocatalytic water treatment, and agricultural antifungal formulations where sustained antimicrobial activity is desired.

Table 2: Zones inhibition of the bioash-doped-ZnO NCs and Bioash on fungi species

Fungal Species	Bioash-doped ZnO NCs (mm)	Bioash (mm)
Trichophyton verrucosum	12.33 ± 0.13^{b}	18.31 ± 0.00^{a}
Trichophyton rubrum	26.41 ± 0.00^{a}	27.66 ± 0.00^{a}
Trichophyton soudanense	15.37 ± 0.00^{b}	26.31 ± 0.12^{a}
Trichophyton tonsurans	18.77 ± 0.22^{b}	25.67 ± 0.00^{a}
Trichophyton violaceum	10.11 ± 0.40^{b}	19.55 ± 0.00^{a}
Microsporum canis	10.88 ± 0.00^{b}	13.13 ± 0.00^{a}
Trichophyton schoenleinii	26.33 ± 0.00^{b}	30.87 ± 0.00^{a}
Trichophyton mentagrophytes	26.80 ± 0.20^{a}	28.60 ± 0.00^{a}

Values are expressed as mean ± SD (n = 3). Means within a row bearing different superscript letters (a,b) are significantly different at $p < 0.05$ according to Student's t-test. Overall paired t-test comparison between Bioash-doped ZnO NCs and Bioash showed a significant difference ($t = 3.73$, $p = 0.007$).

IV. CONCLUSION

In conclusion, this study successfully demonstrated that oil palm fingers bioash (OPfBA), a low-cost agricultural waste, serves as an effective multi-element dopant and mesoporous support for ZnO Nanocomposites, yielding a structurally integrated hybrid nanocomposite with broad-spectrum antifungal activity against eight clinically relevant dermatophyte species. The dual antifungal mechanism — combining direct ion-mediated membrane disruption from the mineral-rich bioash with reactive oxygen species generation from defect-engineered ZnO — produced inhibition zones (up to 26.80 mm for doped ZnO NCs and 30.87 mm for bioash) that rival conventional antifungals, offering a viable alternative amid rising drug resistance. The valorization of oil palm biomass waste into a functional nanomaterial directly advances several United Nations Sustainable Development Goals, particularly SDG 3, 9,12, and 13. This

work therefore establishes a sustainable, circular-economy paradigm in which agro-industrial waste is transformed into multifunctional nanomaterials that simultaneously address public health, environmental remediation, and industrial innovation challenges.

ACKNOWLEDGEMENTS

We wish to the Centre for Research, Innovation and development (CRID), Federal Polytechnic Ado-Ekiti; for facilitating this study through the Institution-Base Research Fund (IBR-TETFund), 2024. Appreciation also goes to Mr. Isa Yakubu, of the Department of Chemical Engineering, Ahmadu Bello University, Zaria; for assisting in the provision of equipment for analysis. Technologists in the Department of Applied Chemistry, Federal Polytechnic Ado-Ekiti are also appreciated, for their support in making the work fruitful.

REFERENCES

[1] F. Branda, N. Petrosillo, G. Ceccarelli, M. Giovanetti, A. De Vito, G. Madeddu, F. Scarpa, and M. Ciccozzi, "Antifungal agents in the 21st century: Advances, challenges, and future perspectives," Infectious Disease Reports, vol. 17, no. 4, p. 91, 2025, doi: 10.3390/idr17040091.

[2] D. J. Agbadamashi and C. L. Price, "Novel strategies for preventing fungal infections—Outline," Pathogens, vol. 14, no. 2, p. 126, 2025, doi: 10.3390/pathogens14020126.

[3] S. K. Mondal, S. Chakraborty, S. Manna, and S. M. Mandal, "Antimicrobial nanoparticles: Current landscape and future challenges," RSC Pharmaceutics, vol. 1, no. 3, pp. 388–402, 2024, doi: 10.1039/D4PM00032C.

[4] K. P. Greeshma, R. T. Selvi, R. Aiswarya, S. Muthulingam, D. B. Sen, and S. John, "Sustainable ZnO NPs for a greener future: An integrative review of emerging frontiers in environmental, biomedical, and nanoinformatics applications," Biomedical Materials & Devices, pp. 1–28, 2025, doi: 10.1007/s44174-025-00624-7.

[5] D. Rajendran et al., "Comprehensive characterization and biological and safety evaluation of zinc oxide–curcumin nanoconjugates: Unraveling synergistic effects for enhanced therapeutic applications," ACS Omega, vol. 10, no. 25, pp. 27045–27057, 2025, doi: 10.1021/acsomega.5c02224.

[6] M. T. Yassin, F. O. Al-Otibi, A. A. Al-Askar, and M. M. Elmaghrabi, "Synergistic anticandidal effectiveness of greenly synthesized zinc oxide nanoparticles with antifungal agents against nosocomial candidal pathogens," Microorganisms, vol. 11, no. 8, p. 1957, 2023, doi: 10.3390/microorganisms11081957.

[7] A. Lipovsky, Y. Nitzan, A. Gedanken, and R. Lubart, "Antifungal activity of ZnO nanoparticles—The role of ROS mediated cell injury," Nanotechnology, vol. 22, no. 10, p. 105101, 2011, doi: 10.1088/0957-4484/22/10/105101.

[8] S. Djearamane et al., "Antifungal properties of zinc oxide nanoparticles on Candida albicans," Coatings, vol. 12, no. 12, p. 1864, 2022, doi: 10.3390/coatings12121864.

[9] Z. Ding, Q. He, Z. Ding, C. Liao, D. Chen, and L. Ou, "Fabrication and performance of ZnO doped tantalum oxide multilayer composite coatings on Ti6Al4V for orthopedic application," Nanomaterials, vol. 9, no. 5, p. 685, 2019, doi: 10.3390/nano9050685.

[10] M. Hasan, Q. Liu, A. Kanwal, T. Tariq, G. Mustafa, S. Batool, and M. Ghorbanpour, "A comparative study on green synthesis and characterization of Mn doped ZnO nanocomposite for antibacterial and photocatalytic applications," Scientific Reports, vol. 14, no. 1, p. 7528, 2024, doi: 10.1038/s41598-024-58393-0.

[11] M. C. Ogwuegbu, O. C. Olatunde, T. M. Pfukwa, D. M. Mthiyane, O. A. Fawole, and D. C. Onwudiwe, "Green synthesis, characterization and antimicrobial activity of ZnO and Co-doped ZnO nanoparticles obtained using aqueous extracts of Platycladus orientalis leaves," Discover Materials, vol. 5, no. 1, p. 55, 2025, doi: 10.1007/s43939-025-00230-w.

[12] J. Gautam, A. M. Kale, J. Rawal, P. Varma, S. J. Lee, S. Y. Lee, and S. J. Park, "Biomass-derived carbon photocatalysts for organic pollutant degradation: Strategies and perspectives," Carbon Neutralization, vol. 5, no. 1, p. e70109, 2026, doi: 10.1002/cnl2.70109.

[13] A. I. Oliva, I. J. González-Chan, P. E. Várguez, A. I. Trejo-Ramos, and A. I. Oliva-Avilés, "The chemical process for materials deposition in aqueous solution: A review," Surface Engineering, vol. 38, nos. 10–12, pp. 907–929, 2022, doi: 10.1080/02670844.2023.2187883.

[14] B. Tiss, D. Martínez-Martínez, B. Silva, N. Bouguila, L. El Mir, B. Almeida, C. Moura, and L. Cunha, "Growth of Al:ZnO nano-flowers by pulsed laser ablation deposition," Optics & Laser Technology, vol. 174, p. 110673, 2024, doi: 10.1016/j.optlastec.2024.110673.

[15] F. L. Koao, F. B. Dejene, C. H. Swart, V. S. Motloung, E. T. Motaung, and P. S. Hlangothi, "Effect of Tb^{3+} ions on the ZnO nanoparticles synthesized by chemical bath deposition method," Advanced Materials Letters, vol. 7, no. 7, pp. 529–535, 2016, doi: 10.5185/amlett.2016.6128.

[16] E. C. Oroke, F. I. Nwabue, and F. S. Nworie, "Equilibrium, kinetic and thermodynamic studies of an Elaeis guineensis fingers biochar-doped ZnO nanoparticles prepared using chemical bath deposition technique," Tech-Sphere Journal for Pure and Applied Science, vol. 1, no. 1, pp. 1–18, 2024.

[17] M. Mazher, M. Anjum, W. Mushtaq, Q. Noshad, and N. Z. Malik, "Antifungal assay of Solanum nigrum Linn. fruit, leaves and stems extracts in different solvents," International Journal of Biosciences, vol. 10, no. 4, pp. 380–385, 2017, doi: 10.12692/ijb/10.4.380-385.

[18] S. H. Sumrra, A. U. Hassan, W. Zafar, Z. H. Chohan, and K. A. Alrashidi, "Molecular engineering for UV-Vis to NIR absorption/emission bands of pyrazine-based A-π-D-π-A switches to design TiO_2 tuned dyes: DFT insights," Journal of Fluorescence, vol. 35, no. 7, pp. 5457–5474, 2025, doi: 10.1007/s10895-024-03891-7.

[19] I. K. Maurya et al., "Antifungal activity of novel synthetic peptides by accumulation of reactive oxygen species (ROS) and disruption of cell wall against Candida albicans," Peptides, vol. 32, no. 8, pp. 1732–1740, 2011, doi: 10.1016/j.peptides.2011.06.003.

[20] M. Casa, M. Sarno, L. Paciello, M. R. Beaumont, and P. Ciambelli, "Synthesis and characterization of water stable ZnO quantum dots based-sensor for nitro-organic compounds," Chemical Engineering Transactions, vol. 47, pp. 7–12, 2016, doi: 10.3303/CET1647002.

[21] P. Mondal, "Effect of oxygen vacancy induced defect on the optical emission and excitonic lifetime of intrinsic ZnO," Optical Materials, vol. 98, p. 109476, 2019, doi: 10.1016/j.optmat.2019.109476.

[22] M. S. Khan et al., "Insight into the electronic, optical and transport nature of Al_2CdX_4 (X = S, Se and Te) employing the accurate mBJ approach: Novel materials for opto-electronic devices," Materials Science in Semiconductor Processing, vol. 135, p. 106098, 2021, doi: 10.1016/j.mssp.2021.106098.

[23] J. Islam and A. A. Hossain, "Narrowing band gap and enhanced visible-light absorption of metal-doped non-toxic $CsSnCl_3$ metal halides for potential optoelectronic applications," RSC Advances, vol. 10, no. 13, pp. 7817–7827, 2020, doi: 10.1039/C9RA10407K.

[24] H. S. Bolarinwa et al., "Determination of optical parameters of zinc oxide nanofibre deposited by electrospinning technique," Journal of Taibah University for Science, vol. 11, pp. 1245–1258, 2017, doi: 10.1016/j.jtusci.2017.01.004.

[25] Y. Hu, "Two-dimensional molybdenum oxide in optical applications," Ph.D. dissertation, RMIT Univ., Melbourne, Australia, 2023, doi: 10.25439/rmt.28322024.

[26] C. Belabed, B. Bellal, A. Tab, K. Dib, and M. Trari, "Optical and dielectric properties for the determination of gap states of the polymer semiconductor: Application to photodegradation of organic pollutants," Optik, vol. 160, pp. 218–226, 2018, doi: 10.1016/j.ijleo.2018.01.109.

[27] X. Jiang, K. A. Whitehead, N. Arneborg, Y. Fang, and J. Risbo, "Understanding bacterial surface and adhesion properties and the implications for Pickering stabilization of colloidal structures," Current Opinion in Colloid & Interface Science, vol. 69, p. 101767, 2024, doi: 10.1016/j.cocis.2023.101767.

[28] A. Mohammad, H. A. Al-Jafa, H. S. Ahmed, M. Mohammed, and Z. Khodair, "Structural and morphological studies of ZnO nanostructures," Journal of Ovonic Research, vol. 18, no. 3, pp. 443–452, 2022, doi: 10.15251/JOR.2022.183.443.

[29] B. Abebe, E. A. Zereffa, A. Tadesse, and H. A. Murthy, "A review on enhancing the antibacterial activity of ZnO: Mechanisms and microscopic investigation," Nanoscale Research Letters, vol. 15, no. 1, p. 190, 2020, doi: 10.1186/s11671-020-03418-6.

[30] V. Amrute, K. K. Supin, M. Vasundhara, and A. Chanda, "Observation of excellent photocatalytic and antibacterial activity of Ag doped ZnO nanoparticles," RSC Advances, vol. 14, no. 45, pp. 32786–32801, 2024, doi: 10.1039/D4RA05197A.

[31] D. Thapliyal, G. D. Verros, and R. K. Arya, "Nanoparticle-doped antibacterial and antifungal coatings," Polymers, vol. 17, no. 2, p. 247, 2025, doi: 10.3390/polym17020247.

[32] R. O. Kareem, A. A. Barzinjy, T. Ates, N. Bulut, S. Keser, and O. Kaygili, "Advances in metallic ion-doped hydroxyapatite: Unlocking enhanced structural, biological, and functional properties for cutting-edge biomedical applications," Journal of the Australian Ceramic Society, pp. 1–33, 2025, doi: 10.1007/s41779-025-01289-7.

[33] J. Zhou, S. Hao, Y. Chen, S. Zhang, and W. Xu, "Multiscale investigation of thermally activated coal gangue aggregate concrete interfacial transition zone evolution and failure mechanisms," Scientific Reports, vol. 15, no. 1, p. 28663, 2025, doi: 10.1038/s41598-025-14014-y.

[34] P. Muhammad et al., "Defect engineering in nanocatalysts: From design and synthesis to applications," Advanced Functional Materials, vol. 34, no. 29, p. 2314686, 2024, doi: 10.1002/adfm.202314686.

[35] V. G. Baldovino-Medrano, V. Niño-Celis, and R. Isaacs Giraldo, "Systematic analysis of the nitrogen adsorption–desorption isotherms recorded for a series of materials based on microporous–mesoporous amorphous aluminosilicates using classical methods," Journal of Chemical & Engineering Data, vol. 68, no. 9, pp. 2512–2528, 2023, doi: 10.1021/acs.jced.3c00257.

[36] J. P. Usliyanage, G. Perera, G. Thiripuranathar, and F. Menaa, "Synthetic strategies of Ag-doped ZnO nanocomposites: A comprehensive review," Biomass Conversion and Biorefinery, vol. 15, no. 1, pp. 19–39, 2025, doi: 10.1007/s13399-023-05139-z.

[37] I. A. Mir, V. S. Radhakrishanan, K. Rawat, T. Prasad, and H. B. Bohidar, "Bandgap tunable AgInS-based quantum dots for high contrast cell imaging with enhanced photodynamic and antifungal applications," Scientific Reports, vol. 8, no. 1, 2018, doi: 10.1038/s41598-018-27246-y.

[38] C. Leeyaphan et al., "Efficacy, safety, and cost-effectiveness of zinc oxide nanoparticles in Whitfield's spirit solution for treating superficial fungal foot infections: A randomized controlled trial," Dermatology and Therapy, vol. 15, no. 2, pp. 351–365, 2025, doi: 10.1007/s13555-025-01340-2.